Journal of The Electrochemical Society, **152** (8) A1606-A1612 (2005)
0013-4651/2005/152(8)/A1606/7/$7.00 © The Electrochemical Society, Inc.

Microfabricated Fuel Cells with Thin-Film Silicon Dioxide Proton Exchange Membranes

Christopher W. Moore,* Jun Li,* and Paul A. Kohl,z**

School of Chemical and Biomolecular Engineering, Georgia Institute of Technology, Atlanta, Georgia 30332, USA

Microfabricated fuel cells have been designed and constructed on silicon integrated circuit wafers using many processes common in integrated circuit fabrication, including sputtering, polymer spin coating, reactive ion etching, and photolithography. Proton exchange membranes (PEMs) for an "integrated" fuel cell have been made by low-temperature, plasma-enhanced chemical vapor deposition of silicon dioxide. Fuel delivery channels were made through the use of a patterned sacrificial polymer below the PEM and anode catalyst. Platinum-ruthenium catalyst was deposited by dc sputtering. The resistivity of the oxide films was higher than traditional polymer electrolyte membranes, e.g., Nafion, but they were also much thinner. Thus, the "area-resistance" (product of resistivity times thickness) was similar. Fuel cell performance shows that the amount of catalyst in the thin-film electrodes chiefly limits the performance. Steady-state power densities of 30 μW at 0.3 V were achieved for a double-layer sputtered anode catalyst device with hydrogen fuel at room temperature.
 [DOI: 10.1149/1.1949027]

Manuscript submitted November 23, 2004; revised manuscript received March 13, 2005. Available electronically July 7, 2005.

Portable electronic devices, including those for mobile communications, microsensors, microelectromechanical systems (MEMS), and microfluidic devices will benefit from advances in energy storage. The availability of power sources with higher energy density and lower cost will enable a wider range of usage and functionality. One possible higher energy density source is the fuel cell.

For electronic devices with small power requirements, microfabricated power sources, including fuel cells, are being investigated.[1-6] The possibility of cofabricating a power source on the same substrate as the electric circuit offers many advantages, including a reduction in size and weight, improved signal integrity because of fewer interconnects, increased processing efficiency, and lower cost. Integrated microfabricated fuel cells are potentially the smallest form-factor chemical energy source with the lowest cost because they use materials and processes already present in the electronic device.

Two of the fuels of interest in these microfuel cells for consumer devices are hydrogen and methanol. Hydrogen fuel cells and direct methanol fuel cells (DMFCs) are operated at relatively low temperature, e.g., ambient to 120°C. They employ a solid proton exchange membrane (PEM) to transport the protons from the anode to the cathode. Hydrogen can be stored as a pressured gas or in a metal hydride form. It requires humidification for high membrane conductivity. A methanol-water mixture can be oxidized at the anode in either liquid or vapor form. Methanol is an attractive fuel because it can be stored as a liquid, is inexpensive, and has a high specific energy.[7-9] Compared with other fuel cell systems, the liquid-feed DMFC is relatively simple and could be easily miniaturized because it does not need a fuel reformer, complicated humidification, or a thermal management system.[10-12] Furthermore, methanol has a high energy density in comparison with lithium polymer and lithium-ion polymer batteries.[13]

PEMs can be used in low-temperature fuel cells that operate with either hydrogen or methanol.[14] The solid membrane in conventional fuel cells is usually a perfluorinated polymer with sidechains terminating in sulfonic acid moieties, such as Nafion. Membranes in PEM fuel cells generally contain water to keep the conductivity high. Methanol crossover causes a mixed potential and poisoning of the oxygen reduction reaction,[15] leading to decreased performance.

Compared to conventional fuel cells, a PEM in a microfabricated fuel cell should be thin to match the thickness of the other materials, such as insulators on electronic devices. The use of an alternate membrane material with a higher resistance to methanol crossover and less dependence on water concentration is desired for thin-film membranes. The ionic conductivity, however, may be lower for the thinner film, resulting in a similar "area resistance," which is the product of resistivity and film thickness. The deposition temperature of plasma-enhanced chemical vapor deposition (PECVD) silicon dioxide has been shown to have a large effect on silanol and water concentrations in the film, leading to increased polarity and therefore higher ionic conductivity.[16] The resistance to methanol permeation through inorganic glasses is very high. In addition, the mechanical properties make it suitable for use in the thin-film design being used, making it an attractive alternative to be studied.

Another important topic to investigate in microfabricated fuel cells is decreased catalyst loading. Pt-Ru alloy catalysts are the most efficient anode catalysts for methanol electro-oxidation.[17-19] The addition of Ru to the Pt catalyst enhances the rate of methanol electro-oxidation because the Ru provides a site for water oxidation and OH adsorption needed in oxidation of methanol to CO_2. The availability of adsorbed OH on the Ru lowers the number of CO intermediates on the Pt.[20-23] In a typical DMFC, the anode catalysts are generally present in the form of nanoparticles supported on high-surface-area carbon in contact with the membrane.[20,24-26] Sputtering the metal catalyst allows for very low catalyst loading because of the size of the deposited particles in the island growth stage of film deposition. The advantages to sputtering the catalyst include the lower Pt loading[27] because of the higher surface area to weight ratio and a reduction in methanol crossover due to better coverage.[28] Depositing a single layer of catalyst onto the membrane limits the amount of catalyst that can be deposited, because the film must remain porous to allow reactants to contact as much of the catalyst at the catalyst/electrolyte interface. The anode reaction must occur at the interface between the catalyst and electrolyte membrane for the protons to be transported to the cathode, where they subsequently are consumed in the cathode reaction where the membrane and catalyst are in contact. A fabrication technique that can increase the amount of sputtered catalyst while maintaining porosity for reactant access to the membrane can be an important factor in improving cell performance.

Using an ionically conductive fuel expands the effective surface area within the anode chamber that can be used for catalysis. Adding an acid to methanol fuel has been shown to improve performance in anode designs that are limited by the catalytic activity.[29] An acidic methanol solution serves as the fuel and a proton transport medium to the membrane from Pt-Ru catalyst lining the anode chamber not in contact with the electrolyte membrane. The acid solution, which makes use of all of the catalyst in the anode chamber (including catalyst not directly on the membrane), produces higher current den-

* Electrochemical Society Student Member.
** Electrochemical Society Fellow.
z E-mail: paul.kohl@chbe.gatech.edu

sity than the methanol and water solution that can only deliver protons to the membrane that are generated on the catalyst in direct contact with the membrane.

In this work, microchannel-based fuel cells employing silicon dioxide as the PEM and sputtered layers of Pt/Ru catalyst were fabricated and tested. Half-cell and full-cell measurements with hydrogen, methanol, and acidic methanol have been performed. Results are presented to demonstrate the effectiveness of the materials and design presented, with emphasis given to the catalytic activity of the anode.

Experimental

The design and fabrication of the microfuel cells is based on a technique of using a sacrificial polymer to form the fuel delivery channels for the anode.[30] This sacrificial polymer, Unity 2000P (Promerus LLC, Brecksville, OH), was patterned by ultraviolet exposure and thermal decomposition of the exposed areas.[31] The membrane and electrodes coat the patterned features in a sequential buildup process. One of the last steps in the fabrication sequence is the thermal decomposition of the patterned Unity features, leaving encapsulated microchannels. Figure 1 shows the process sequence for fabricating the enclosed air gaps, or microchannels, in an encapsulating material. Unity decomposition took place in a Lindberg tube furnace with a steady nitrogen flow. The final decomposition temperature and time was 170°C for 1.5 h. The microfuel cell fabrication included deposition of catalytic electrodes and current collectors before and after the encapsulating material, which served as the PEM, was deposited. A schematic cross section of the device built on an array of parallel microchannels is shown in Fig. 2.

Silicon dioxide was used as the encapsulating material and PEM. The deposition of SiO_2 took place in a Plasma-Therm PECVD system (Plasma-Therm, St. Petersburg, FL) at temperatures of 60-200°C. The reactant gases were silane and nitrous oxide with a N_2O:SiH_4 ratio of 2.25 and operating pressure of 600 mTorr. Deposition times of 60-75 min produced film thicknesses, measured with an Alpha-Step surface profilometer (KLA-Tencor, San Jose, CA), between 2.4 and 3.4 μm.

The catalyst layers were sputter deposited using a CVC dc sputterer (CVC Products, Inc., Rochester, NY). A 50:50 atomic ratio platinum/ruthenium target (Williams Thin-Film Products, Brewster, NY) was used as the source target. X-ray photoelectron spectroscopy (XPS) confirmed that the sputtered films had equal amounts of the two metals. Porous films with average thicknesses of 50-200 Å were deposited on the sacrificial polymer, and then coated with the membrane, to serve as anode catalysts. In addition, a 600-Å-thick layer of Pt/Ru was deposited on the bottom of the anode microchannels opposite the membrane to serve as both additional catalyst and for current collection. This additional catalyst improved the performance of the microchannel fuel cells, particularly when using acidic methanol.

Porous catalytic cathodes were also fabricated by sputtering of Pt or Pt/Ru on the top, or outside, of the PEM. However, the cathodes on some samples were made by painting a prepared catalyst ink containing carbon-supported Pt in Nafion on the PEM, followed by coating with a porous gold current collector. This thick-film approach increased the catalyst loading and performance on the cathode side of the PEM. This was especially useful in studying the anode performance by eliminating the oxygen reduction at the cathode from being the rate-limiting step.

All electrochemical measurements, including impedance spectroscopy (IS) and linear voltammograms, were performed with a Perkin Elmer PARSTAT 2263 (EG&G, Princeton, NJ) electrochemical system. The scan rate for linear sweep voltametry was 1 mV/s. Ionic conductivity was measured with IS through SiO_2 films deposited onto aluminum-coated substrates and contacted with a mercury probe, as well as with actual cells. The frequency range for the impedance measurement was from 100 mHz to 1 MHz, with an ac signal amplitude of 10 mV. Half-cell devices were fabricated with the fuel delivery channels and sputtered catalyst under the SiO_2

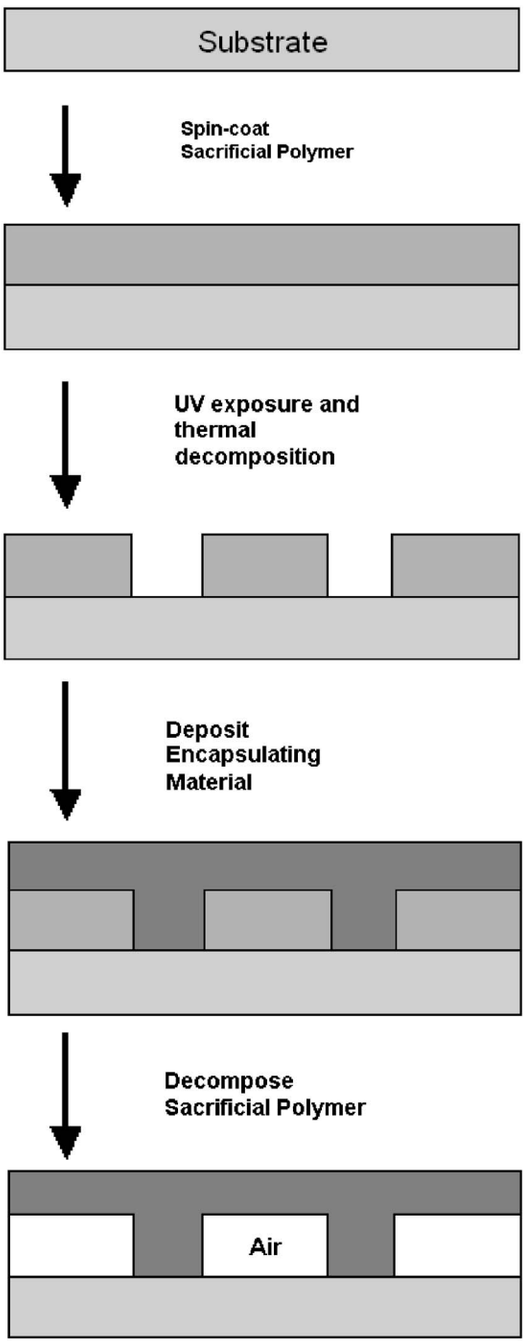

Figure 1. Microchannel formation process using photodefinable PPC.

PEM. Instead of a cathode, epoxy was used to form a well on top of the devices and filled with a 1 M sulfuric acid solution. Measurements were made with a saturated calomel electrode (SCE) and a Pt wire as the reference and counter electrodes, respectively, placed in the sulfuric acid solution. A PHD 2000 programmable syringe pump (Harvard Apparatus, Holliston, MA) delivered liquid fuels and controlled the flow rates. Hydrogen was supplied with a pressurized tank of ultrahigh-purity-grade gas that passed through a bubbler to humidify the feed.

Results and Discussion

Microfabricated fuel cells were successfully fabricated using many materials and processes common to integrated circuit fabrica-

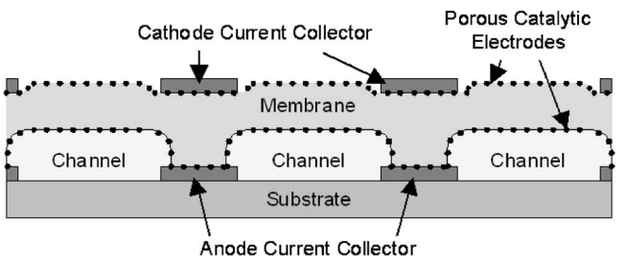

Figure 2. Cross section of a thin-film fuel cell with parallel microchannels.

tion. The performance of the microfuel cells with different fuels and temperatures was measured for cells with different features, including half cells and full cells. The purpose was to investigate the individual fuel cells' components (anode, cathode, and PEM) as a function of processing conditions.

In addition to catalytic activity, the key properties that were desired for the sputtered catalyst layers were porosity and electrical conductivity. The catalyst layer that contacts the membrane must be porous so that the protons generated during oxidation can come in contact with the PEM and pass to the cathode. The electrons generated at the anode catalyst need a path to the metal current collectors. To test the sheet resistance of sputtered Pt films, different amounts of Pt were sputtered onto substrates containing two solid electrodes patterned on top of an oxide film with a space between them. The sheet resistance of the Pt layers across the space between the electrodes was measured. Figure 3 shows the measured resistance ($\Omega/\square$) of sputtered Pt films as a function of thickness and the calculated values for smooth, continuous films of the indicated thickness. Above 300 Å the measured values correspond to the expected values, indicating that the films were contiguous. Below 150 Å the resistance increased more dramatically with decreasing thickness. This corresponded to a porous, discontinuous film, which was desired. Roughening of the Unity sacrificial polymer's surface through reactive ion etching (RIE) increased the amount of metal that could be sputtered before making a solid layer. In this work, Pt/Ru layers with an average thickness of 50-200 Å were used as porous, conducting layers on roughened Unity.

Because SiO_2 does not adhere well to Pt/Ru, it was necessary to deposit a titanium adhesion layer on top of the Pt/Ru before SiO_2 deposition. The amount of Ti needed for adhesion was minimized in order to maximize the interface area of the catalyst and electrolyte.

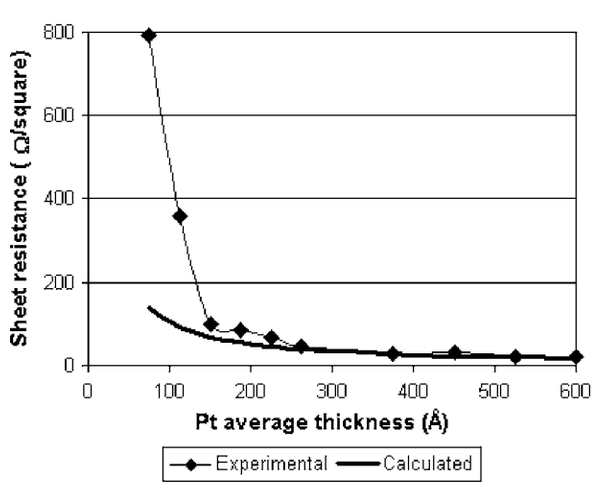

Figure 3. Measured and calculated resistances for sputtered platinum films.

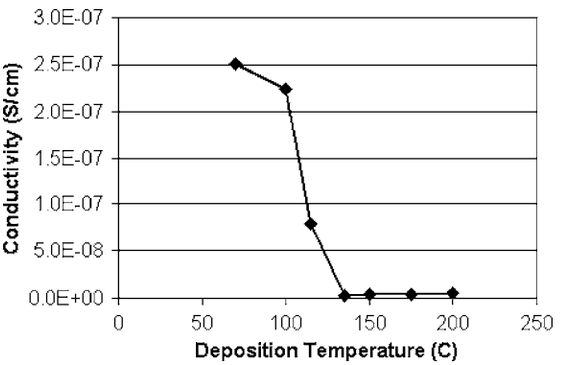

Figure 4. Ionic conductivity of SiO_2 films measured through impedance spectroscopy.

It was found that 45 Å (average thickness) of Ti was necessary between Pt/Ru and SiO_2 in the sputtered electrodes. Less titanium resulted in poor adhesion.

Sputtering 600 Å, or approximately 100 $\mu g/cm^2$, of Pt/Ru prior to the deposition and patterning of the Unity sacrificial polymer produced a relatively solid (nonporous) layer on the substrate that increased the total amount of anode catalyst in the cell that could be utilized by a conducting analyte (acidic methanol). It also seemed to marginally improve performance with hydrogen. Therefore, all reported results are for cells fabricated with a solid layer of Pt/Ru on the bottom of the microchannels.

The requirements for the PEM are different from the traditional PEM, e.g., Nafion, due to the mechanical properties and thickness required in microfabricated fuel cells. Here, SiO_2 is shown to work as a stand-alone membrane. SiO_2 films were deposited by PECVD and the ionic conductivity was measured through the use of impedance spectroscopy at room temperature. Figure 4 shows the ionic conductivity of silicon dioxide vs deposition temperature. As the deposition temperature decreased, the conductivity increased due to higher silonol concentration and lower density.[16] The conductivity of the films was much lower than for other commonly used PEMs, such as Nafion, but they are also much thinner than other fuel cell membranes. Extruded Nafion membranes (equivalent weight of 1100) have area resistances of 0.1-0.35 $\Omega\ cm^2$.[32] The area resistance of a 3 μm thick SiO_2 film deposited at 100°C is 1200 $\Omega\ cm^2$ at room temperature. The relatively high resistance leads to a decrease in cell voltage at higher current. The SiO_2 films used in these devices were adequate to investigate the other parameters, such as the anode and cathode catalyst loading. While they are sufficient for the lower current devices used in this study, improved SiO_2 PEMs are being investigated and will be reported in the future.

Half-cell devices were fabricated and tested to evaluate the anode performance with different fuels and provide a comparison for the full-cell tests. Figures 5 and 6 show the half-cell results for hydrogen and methanol, respectively. A solid layer of Pt/Ru was deposited before the sacrificial polymer was patterned, as well as a porous layer on top of the patterned features to be in contact with the membrane. The catalyst weight at the membrane surface was 17 $\mu g/cm^2$.

Hydrogen was supplied with a pressurized tank of ultrahigh-purity grade gas that passed through a bubbler to humidify the feed. Figure 5 shows the results for inlet pressures of 1-4 psig (15.7-18.7 psia). The current densities of the half-cells scale with the partial pressure of the humidified hydrogen. This indicates that the performance is chiefly limited by the mass transfer of dissolved hydrogen molecules at the anode and is therefore proportional to hydrogen partial pressure. Further improvements in current density are possible with improved activity of the anode catalyst.

The methanol in water concentration was 1 M. The acidic methanol mixture contained 1 M sulfuric acid with 1 M methanol. Figure

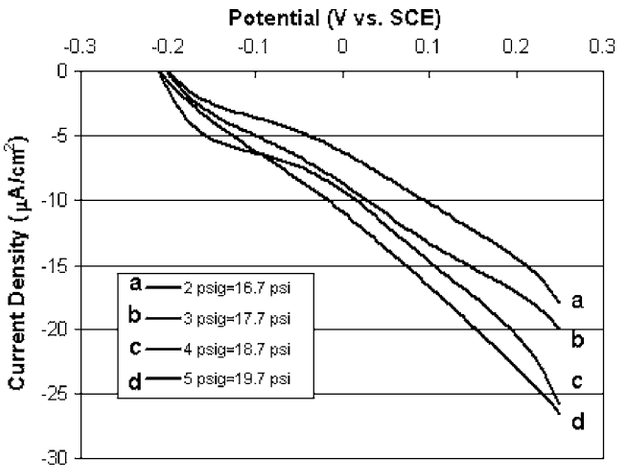

Figure 5. Half-cell performance of microchannels with humidified hydrogen.

6 shows the half-cell polarization curves for methanol and acidic methanol. Adding sulfuric acid to the fuel made the solution conductive to protons. The increase in utilized catalyst area, due to the conductivity of the acidic methanol solution, improved the current density. The Pt/Ru catalyst that was deposited on the walls of the channel not in contact with the membrane was utilized to increase the amount of methanol oxidation. Increasing the flow rate of the acidic methanol fuel improves the current density and open-circuit potential. The main detriment to performance at lower flow rates appears to be the formation of carbon dioxide bubbles at the anode that must be pushed out of the microchannels. With the current densities observed at 0.25 V vs SCE (2 and 7 mA/cm^2 for 1 and 5 mL/h, respectively), the production of gaseous CO_2 bubbles cover catalyst sites and may also restrict the proton conductance through the fuel from the bottom of the microchannels to the PEM.

Microfabricated full cells were fabricated and tested with linear voltammetry at a scan rate of 1 mV/s from the open-circuit potential. Table I compares the differences in process between five sets of cells that are presented here to demonstrate the key parameters (anode and cathode construction) that affect cell performance for these power devices.

Figure 7 shows polarization (top) and power (bottom) curves for one cell, sample A, which had sputtered catalyst with a loading of 31 μg/cm^2 at both the anode and cathode. Humidified hydrogen with an inlet pressure of 1 psig served as the fuel and oxygen from the air was reduced at the cathode. The performance at 60°C was approximately four times greater than at ambient conditions, with a measured peak power density of 4 μW/cm^2. The lower current densities of these devices with sputtered catalyst on the cathodes compared to the results from the anode half-cells run with hydrogen shown in Fig. 5 demonstrate that their performance is limited by the catalytic activity of the air cathode. This agrees with the expectation that ambient oxygen reduction at the cathode would be performance limiting when pressurized hydrogen was used at the anode.

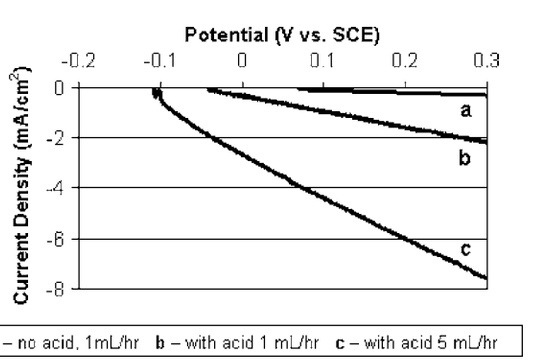

Figure 6. Half-cell performance of microchannels with methanol-water and acid-methanol-water solutions.

Table I. Processing characteristics of microfuel cell samples.

Sample	Anode catalyst weight[a] (μg/cm^2)	SiO_2 membrane thickness (μm)	Cathode catalyst
A	31	3.2	Sputtered
B	17	3.2	Thick-film
C	34	3.2	Thick-film
D	43[b]	3.2	Thick-film
E	17	2.4	Thick-film

[a] Weight at membrane surface (100 μg/cm^2 at bottom of microchannels)
[b] Total weight of two Pt/Ru layers with 400 Å SiO_2 deposited between

A thick-film ink catalyst was coated onto the air-breathing cathode to improve its area and catalyst activity. When using the painted catalyst ink on top of the membrane, the full-cell performance increased dramatically due to the increase in cathode catalyst loading. Because of the significant improvement to the oxygen reduction at the cathode, it was no longer the limiting electrode. The performance of cells with the thick-film cathode was a function of the anode composition. Figure 8 shows the polarization (top) and power (bottom) curves at ambient temperature, 40°C, and 60°C for sample B. This sample had an anode and membrane similar to sample A, but used the catalyst ink and porous gold current collector for the cathode. Hydrogen with an inlet pressure of 1 psig was the fuel and the cathode was air-breathing. The room-temperature polarization curve

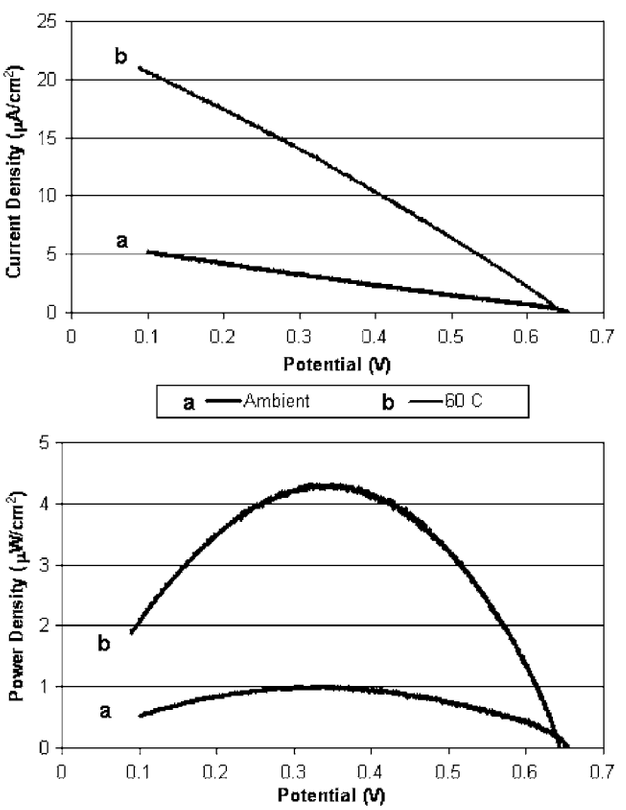

Figure 7. Microfuel cell performance with sputtered anode and cathode.

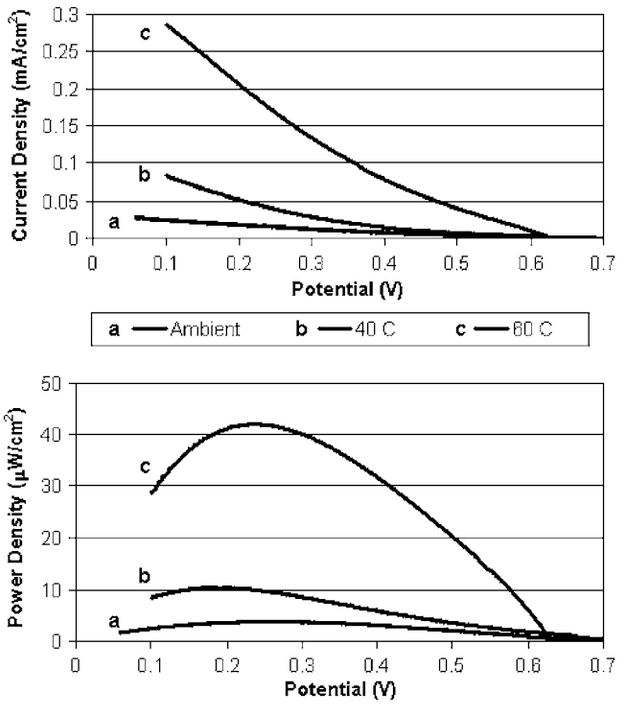

Figure 8. Microfuel cell performance with sputtered anode and thick-film cathode.

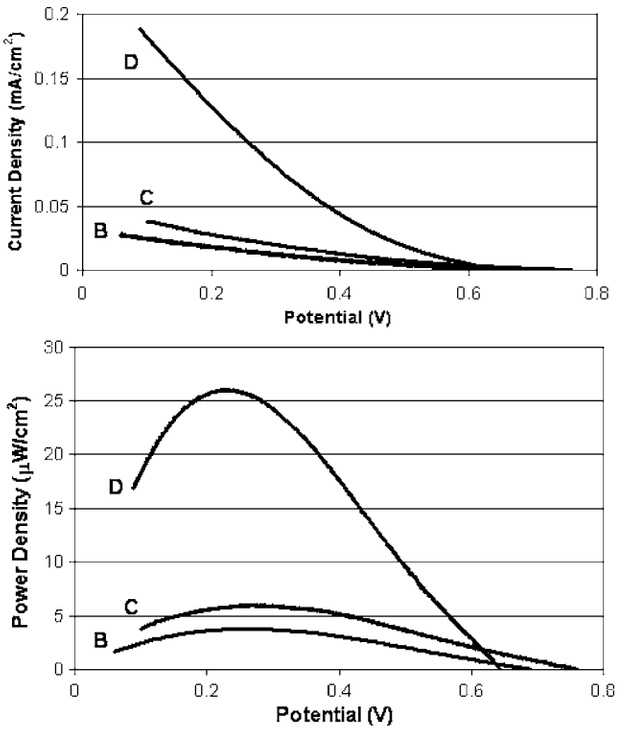

Figure 9. Ambient temperature microfuel cell performance for samples B, C, and D with different amounts of sputtered anode catalyst.

shows current densities very similar to the hydrogen half-cell results from Fig. 5. The performance was approximately one order of magnitude greater than sample A, with a peak power density of 42 $\mu W/cm^2$ at 0.23 V and 60°C. These two results indicate that the anode limits the sample's performance when using the painted catalyst instead of the sputtered catalyst at the cathode.

The temperature dependence was such that greater power output could be achieved at elevated temperatures. Waste heat is produced in fuel cells; however, the size of these devices and the amount of power generated suggest that they would not be able to retain enough heat for operation at an elevated temperature. Integrated fuel cells could also use some heat released from the circuit (or other electronic devices) that they are built on.

Improvements in the activity and surface area of the anode can lead to higher currents and power densities. The anode performance was improved with a higher catalyst loading. Figure 9 shows the room-temperature polarization (top) and power (bottom) curves of three samples with different amounts of sputtered catalyst at the anode. Humidified hydrogen with an inlet pressure of 1 psig was the fuel and the thick-film cathodes were air-breathing. A solid layer of approximately 100 $\mu g/cm^2$ of Pt/Ru was deposited on the bottom of the microchannels on each sample. At the membrane surface, sample B had 17 $\mu g/cm^2$ of Pt/Ru and sample C had 34 $\mu g/cm^2$. With twice as much sputtered Pt/Ru at the membrane, sample C shows an improvement in performance of less than 50% over sample B. Sputtering twice as much Pt/Ru does not double the catalyst surface area because the deposited islands are getting bigger, forming a more continuous (less porous) film.

To improve the electrode performance, the catalyst surface area, particularly the catalyst that is in direct contact with the electrolyte, must be increased. A thin layer of SiO_2 electrolyte could be deposited between two catalyst depositions because it was deposited through PECVD. Sample D had the same 34 $\mu g/cm^2$ catalyst layer as C deposited on the patterned sacrificial polymer, followed by a deposition of 400 Å of SiO_2, and then an additional 8.5 $\mu g/cm^2$ of catalyst, before the thicker SiO_2 PEM layer was deposited. The second layer of sputtered Pt/Ru was imbedded in SiO_2, increasing the catalyst/electrolyte contact area. With only 25% more Pt/Ru at the membrane, the peak power density of sample D was over four times greater than sample C at room temperature. This dramatic improvement in current and power density was due to the SiO_2-encapsulated layer of Pt/Ru that allowed for more membrane/catalyst contact in addition to the increase in total catalyst weight. The two thin layers of Pt/Ru and the small amount of SiO_2 between them most likely form a mixed matrix of catalyst and electrolyte that is conductive to both protons and electrons while increasing the overall catalyst surface area, particularly the area in contact with the electrolyte.

The performance of the hydrogen fuel cells was studied as a function of time to determine if the data collected through linear voltammetry matches steady-state values at constant potential. Figure 10 shows the current density of sample D when a constant potential is held for 10 min. The data show a relatively constant performance that is very close to the values collected for a linear sweep of 1 mV/s, as shown in Fig. 11. Tests over longer periods of time,

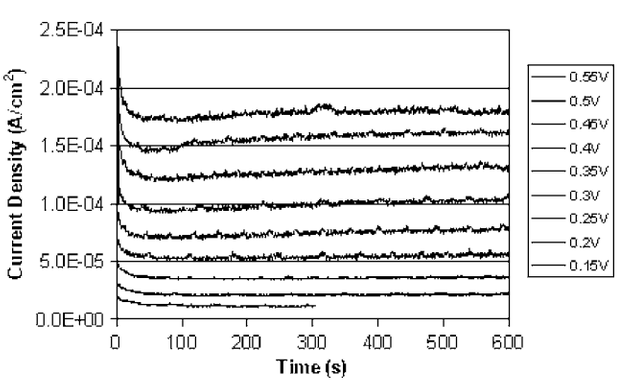

Figure 10. Current density of the imbedded catalyst sample held at constant potential for 10 min.

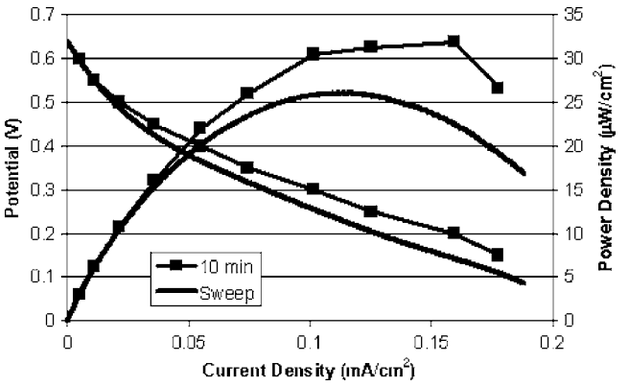

Figure 11. Comparison between steady state (at 10 min) and linear voltammetry polarization data for sample D with humidified hydrogen at room temperature.

such as a few hours, with different devices have shown similar results. The SiO_2 did not swell with water like Nafion films, making them less susceptible to changes with time, such as a drop in performance from drying out.

Figure 12 shows the polarization and power curve for the acidic methanol solution run at room temperature with a flow rate of 1 mL/h in sample E, a microchannel full-cell with the thick-film cathode. The solid layer of catalyst at the bottom of the microchannel is utilized in addition to the porous Pt/Ru at the membrane in the oxidation of methanol because the fuel solution can conduct protons. Compared to the same device operating with hydrogen, the open-circuit potential was lower, but the current and power densities are much higher.

The experiments have shown trends that are being used to further enhance the performance of microfabricated fuel cells. Adding catalyst to the bottom of microchannels is an effective technique for use with conductive fuels. However, increasing the catalyst at the membrane through the use of multiple SiO_2 imbedded layers to maintain porosity shows promise for increased current density.

Additional areas of ongoing study include increased catalyst at the electrodes and improved membrane conductivity. Reducing the thickness of SiO_2 would decrease the resistance of the PEM, but the mechanical strength must be maintained to avoid fuel cells breaking from the pressure of the fuel in the anode microchannels.

Conclusions

Microfuel cells utilizing sacrificial polymer-based microchannels and thin-film SiO_2 membranes have been successfully fabricated and tested. Low-temperature PECVD silicon dioxide shows promise for use in integrated thin-film devices. Lowering the deposition temperature dramatically increased the conductivity of the films to an acceptable level for the current densities achieved with the fabricated electrodes used in this study.

The performance is chiefly limited by the amount of catalyst used. While the current density is acceptable for the catalyst loading being used, increasing the catalyst in the electrode layers, but still maintaining the porosity of the sputtered layers for proton transport, will be the key to increased performance. Repeated alternate catalyst sputtering and SiO_2 deposition steps to build up a catalyst matrix will provide an electrode with increased catalyst and membrane-catalyst contact area. Additional catalyst that is not in contact with the membrane can be utilized when using a conductive analyte, such as acidic methanol.

Improvements to the membrane will also be a key to the viability of these microfabricated fuel cells. The conductivity of the membranes and the open-circuit potentials, particularly with methanol, are too low. The use of acidic methanol also causes damage to the channel, limiting the viable lifetime of the devices. Various techniques to improve these characteristics are currently being studied. Additional work has already produced oxide films with higher conductivity and they are being incorporated into fuel cells. These results will be publicized in the future.

While the performance was shown to increase dramatically with increased temperature, the ability of these devices to maintain an elevated temperature on their own is questionable because of their small size. The amount of waste heat produced by the fuel cells that can be retained will affect their level of performance because of the temperature dependence of the cells. The goal will be a design with maximum insulation for the fuel cells to keep the operating temperature as high as possible. They will most likely find usage in applications where high current or power output is not as important as the high energy density they can offer at any temperature.

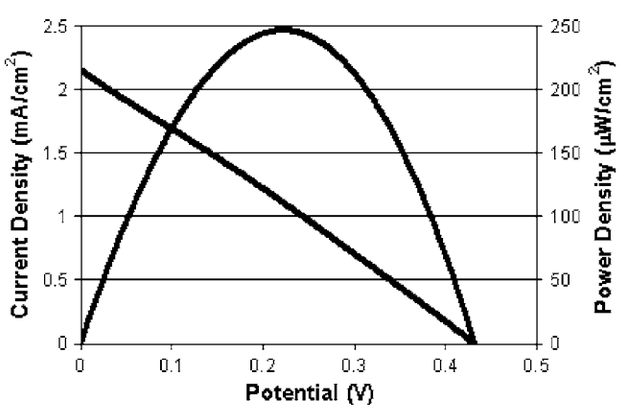

Figure 12. Microchannel full cell performance with 1.0 M acidic methanol at 1 mL/h.

Acknowledgments

The support of the DARPA Micro Power Generation Program is gratefully acknowledged, specifically Dr. Clark Nguyen, program manager. The work is performed under DARPA grant no. F33615-01-1-2173. Also, the help of Dr. Jesse Wainright, Department of Chemical Engineering, Case Western Reserve University, in preparing the catalyst ink and current collector recipes and materials was greatly appreciated.

Georgia Institute of Technology assisted in meeting the publication costs of this article.

References

1. S. C. Kelley, G. A. Deluga, and W. H. Smyrl, *Electrochem. Solid-State Lett.*, **3**, 407 (2000).
2. J. D. Morse, A. F. Jankowski, R. T. Graff, and J. P. Hayes, *J. Vac. Sci. Technol. A*, **18**, 2003 (2000).
3. S. J. Lee, A. Chang-Chien, S. W. Cha, R. O'Hayre, Y. I. Park, Y. Saito, and F. B. Prinz, *J. Power Sources*, **122**, 410 (2002).
4. J. S. Wainright, F. R. Savinell, C. C. Liu, and M. Litt, *Electrochim. Acta*, **48**, 2869 (2003).
5. M. Hayase, T. Kawase, and T. Hatsuzawa, *Electrochem. Solid-State Lett.*, **7**, A231 (2004).
6. J. Yu, P. Chenga, Z. Maa, and B. Yi, *J. Power Sources*, **124**, 40 (2003).
7. L. Carrette, K. A. Friedrich, and U. Stimming, *Fuel Cells*, **1**, 5 (2001).
8. S. Wasmus and A. Kuver, *J. Electroanal. Chem.*, **461**, 14 (1999).
9. L. J. Burcham and I. E. Wachs, *Catal. Today*, **49**, 467 (1999).
10. A. Oedegaard, C. Hebling, A. Schmitz, S. Møller-Holst, and R. Tunold, *J. Power Sources*, **127**, 187 (2004).
11. Z. G. Shao and I. M. Hsinga, *Electrochem. Solid-State Lett.*, **5**, A185 (2002).
12. A. S. Aricò, S. Srinivasan, and V. Antonucci, *Fuel Cells*, **1**, 133 (2001).
13. R. Dillon, S. Srinivasan, A. S. Aricò, and V. Antonucci, *J. Power Sources*, **127**, 112 (2004).
14. S. Gottesfield and T. Zawodzinski, *Advances in Electrochemical Science and Engineering*, Vol. 5, pp. 195–301, Wiley-VCH, New York (1997).
15. J. T. Wang, S. Wasmus, and R. F. Savinell, *J. Electrochem. Soc.*, **143**, 1233 (1996).
16. M. F. Ceiler, Jr., P. A. Kohl, and S. A. Bidstrup, *J. Electrochem. Soc.*, **142**, 2067 (1995).
17. L. Li, P. Cong, R. Viswanathan, F. Qinbai, L. Renxuan, and E. S. Smotkin, *Electrochim. Acta*, **43**, 3657 (1998).

18. A. S. Aricò, P. Cretì, E. Modica, G. Monforte, V. Baglio, and V. Antonucci, *Electrochim. Acta*, **45**, 4319 (2000).
19. Y-C. Liu, X-P. Qiu, Y-Q. Huang, W-T. Zhu, and G-S. Wu, *J. Appl. Electrochem.*, **32**, 1279 (2002).
20. F. Maillard, F. Gloaguen, and J-M. Leger, *J. Appl. Electrochem.*, **33**, 1 (2003).
21. J. M. Leger, *J. Appl. Electrochem.*, **31**, 767 (2001).
22. J. Munk, P. A. Christensen, A. Hamnett, and E. Skou, *J. Electroanal. Chem.*, **401**, 215 (1996).
23. H. Wang, C. Wingender, H. Baltruschat, M. Lopez, and M. T. Reetz, *J. Electroanal. Chem.*, **509**, 163 (2001).
24. S. Wasmus and A. Küver, *J. Electroanal. Chem.*, **461**, 14 (1999).
25. A. K. Shukla, P. A. Christensen, A. J. Dickinson, and A. Hamnett, *J. Power Sources*, **76**, 54 (1998).
26. M. Hogarth, P. Christensen, A. Hamnett, and A. Shukla, *J. Power Sources*, **69**, 113 (1997).
27. R. O'Hayre, S.-J. Lee, S.-W. Cha, and F. B. Prinz, *J. Power Sources*, **109**, 483 (2002).
28. W. C. Choi, J. D. Kim, and S. I. Woo, *J. Power Sources*, **96**, 411 (2001).
29. J. Li, C. W. Moore, and P. A. Kohl, *J. Power Sources*, **138**, 211 (2004).
30. D. Bhusari, H. A. Reed, M. Wedlake, A. M. Padovani, S. A. Bidstrup-Allen, and P. A. Kohl, *J. Microelectromech. Syst.*, **10**, 400 (2001).
31. J. P. Jayachandran, H. A. Reed, H. Zhen, L. F. Rhodes, C. L. Henderson, S. A. Bidstrup-Allen, and P. A. Kohl, *J. Microelectromech. Syst.*, **12**, 147 (2003).
32. S. Slade, S. A. Campbell, T. R. Ralph, and F. C. Walsh, *J. Electrochem. Soc.*, **149**, A1556 (2002).